Controllable Continuous-Wave Nd:YVO_4 self-Raman lasers using intracavity adaptive optics

Ran Li,[1*] Mike Griffith,[2] Leslie Laycock,[2] and Walter Lubeigt[1]

[1]*Centre for Microsystems and Photonics, Department of Electronic & Electrical Engineering, University of Strathclyde, Glasgow, G1 1XW, UK*

[2]*BAE Systems Advanced Technology Centre, West Hanningfield Road, Great Baddow, Chelmsford, CM2 8HN, UK*

**Corresponding author: ran.li@strath.ac.uk*

Received Month X, XXXX; revised Month X, XXXX; accepted Month X, XXXX; posted Month X, XXXX (Doc. ID XXXXX); published Month X, XXXX

A controllable self-Raman laser using an adaptive optics-based control loop featuring an intracavity deformable mirror is reported. This method has the potential to alleviate thermal lensing within the Raman and laser gain media and enable solid-state Raman lasers to reach new power levels. A proof-of-concept experiment using a Nd:YVO_4 self-Raman laser and resulting in 18 % enhancement of the first Stokes output power is reported. Moreover, wavelength selection between two Raman laser outputs ($\lambda = 1109$ nm and $\lambda = 1176$ nm) emanating from the 379 cm^{-1} and 893 cm^{-1} Raman shift of YVO_4 respectively was achieved using this adaptive optics technique.

OCIS Codes: (010.1080) Active or adaptive optics, (140.3550) Lasers, Raman, (140.3580) Lasers, solid-state, (140.3530) Lasers, neodymium, (140.6810) Thermal effects.

http://dx.doi.org/10.1364/OL.99.099999

Stimulated Raman Scattering (SRS) is widely recognized as a practical and efficient approach to extend the spectral coverage of solid-state lasers operating in near infrared and visible spectrum especially when SRS is combined with second harmonic generation or sum frequency generation [1-3]. However, the non-elastic nature of SRS results in the dissipation as heat in the Raman material of a significant portion of energy. This inevitably leads to undesired thermo-optical distortions and impacts the performance of the Raman laser (especially when the Raman crystal is inserted within the laser cavity). This additional thermal lensing scales directly with the Raman laser output power and has been identified as the main limitation in power scaling crystalline Raman lasers operating in the continuous-wave (CW) regime [2,4]. The use of low-loss, low-birefringence synthetic diamond can significantly reduce the effects of SRS-induced thermal lensing in CW Raman lasers [5-7]. In this paper, we propose a method to reduce both the effects of SRS and laser-induced thermal lensing leading to power scaling of crystalline Raman lasers. This method is based on a feedback control loop using adaptive optics (AO) which has been used to optimize the performance of solid-state lasers by compensating for the thermal lens effect within the laser gain medium [8-10].

In this paper, the proof-of-concept implementation of this technique inside a crystalline Raman laser is reported for the first time to our knowledge. A bimorph deformable mirror (DM) was inserted as end-mirror in a self-Raman Nd:YVO_4 laser cavity. In this so-called self-Raman configuration, laser conversion and SRS occurred within the same Nd:YVO_4 crystal which in turn, became subject of intense thermal build-up. Consequently, this self-Raman configuration was believed to be an ideal test-bed to implement this feedback loop. In addition to power enhancement, this AO-based system was also used to control the wavelength of the output beam by selecting the Raman transitions of the YVO_4 crystal used in this laser.

The experimental setup, shown in Fig. 1, was built to optimise the first Stokes output power of the Nd:YVO_4 laser emitting at $\lambda = 1176$ nm. In addition to the intracavity DM, the AO feedback loop included a photodiode sensor to detect the Raman output intensity and a pc-based control program featuring a search algorithm. The 18 mm-diameter DM contained 37 piezoelectric actuators distributed in a radial pattern over an active aperture of 15 mm (see Fig. 2). Individual voltages were supplied to the mirror actuators using a multi-channel digital-to-analog converter and a multi-channel high-voltage amplifier. Using a Shack-Hartmann wavefront sensor-based system, the focusing power of the DM along the x-axis as defined in Fig. 2, was measured to range linearly from -0.74 D to 1.03 D when a voltage of -50 V to 250 V was applied to all actuators respectively. Likewise, the focusing power of the DM along the y-axis ranged from -0.61 D to 1.33 D. The random search algorithm described in [8] was integrated within the control program written using National Instruments Labview. This search algorithm aimed to find the DM shape providing the optimum signal recorded by the photodiode. As described in [11], this algorithm was tailored to reduce the effect of the long term output power variation experienced in this type of high power laser systems. In addition, only the central 7 actuators were used in the algorithm to speed up the search procedure. In this way, the DM shape providing the optimum Raman output intensity was approached by the program. A fiber-coupled laser diode (100 μm core diameter, NA ~ 0.22) capable of producing up to 32 W pump power at λ = 880 nm was used to pump the gain medium. Two plano-convex lenses were used to re-image a 100 μm beam waist at the center of the crystal. An a-cut 20 mm-long (2 mm-diameter), 0.3 at. % doped $Nd:YVO_4$ rod was mounted in a water-cooled copper block and used as laser and Raman gain medium. Its side surfaces were anti-reflection (AR)-coated (reflectivity (R) < 0.1 % @ λ = 1064 & 1109 – 1176 nm; R < 5 % @ λ = 880 nm). A x4 intracavity telescope ensured a ~ 1.5 mm diameter laser spot on the DM to maximise its effects on the intracavity laser field. The four-mirror laser cavity for the fundamental radiation was composed by a flat end-mirror, a concave (radius of curvature (ROC) = 1m) high-reflectivity (HR) mirror (both coated with R > 99.95 % @ λ = 1064 & 1109 - 1176nm), the DM (R > 99.9 % @ λ = 1064 nm) and a strongly-concave (ROC = 0.25 m) output coupler (R > 99.97 % @ λ = 1064 nm, transmission (T) = 1 % @ λ = 1176 nm, T ~ 0.2 % @ λ = 1109 nm). Since the DM was not coated for the first Stokes wavelength, a flat dichroic mirror (R < 1 % @ λ = 1064 nm and R > 99.98 % @ λ = 1109 nm & 1176 nm) was used as an end mirror for the first Stokes Raman laser cavity. This dichroic mirror was placed 380 mm away from the output coupler to optimize the mode-match between the fundamental and Raman laser beams within the $Nd:YVO_4$ crystal. The DM was placed so that its x-axis, as defined in Fig. 2, and the optical propagation axis were contained within the horizontal plane.

With no voltage applied to the DM, the laser was aligned to deliver a maximum Raman output power of 500 mW for an absorbed laser diode pump power of 10.8 W. In this case, the focal length of the first order of the thermal lens (f_{thl}) present in the $Nd:YVO_4$ crystal could be estimated to be ~ 50 mm. Using an ABCD-matrix software, the fundamental transverse mode radius of the fundamental (λ = 1064 nm) and Raman (λ = 1176 nm) laser fields at the centre of the gain medium with and without thermal lensing are shown in Table 1. Only the radius of the Raman field was impacted by thermal lensing with a ~ 20 % increase.

Table 1. TEM_{00} mode radius at the centre of the gain medium for fundamental (λ = 1064 nm) and Raman (λ = 1176 nm) field with and without thermal lensing

	no thermal lensing	with f_{thl} = 50 mm
fundamental laser mode radius along x-axis (μm)	101	101
fundamental laser mode radius along y-axis (μm)	95	95
Raman laser mode radius along x-axis (μm)	102	119
Raman laser mode radius along y-axis (μm)	103	119

Then, a pre-optimisation experiment was undertaken when all actuators were simultaneously adjusted. The Raman laser was found to operate only between 60 V to 180 V corresponding to focusing powers of ~ 0 D to ~ 0.80 D respectively. The mirror shape delivering the optimum Raman output power (550 mW) was obtained for a voltage value of 112.5 V applied to all actuators (i.e. focusing powers of DM along the x and y axes were 0.27 D and 0.50 D respectively). In this way, the TEM_{00} mode radius of the fundamental laser field was increased by ~ 20 % (121 μm along x-axis and 116 μm along y-axis) and resulted in a near-perfect mode matching with the Raman laser field at the centre of the gain medium. The beam quality M^2 factor of the Raman laser output beam was similar for both transverse axes and measured less than 1.1 and 1.4 for the first Stokes output and fundamental laser beam respectively. Using this DM shape, the optical power transfer of the Raman laser was measured (see Fig. 3). Then, an optimisation procedure consisting of 42 actuator changes (which corresponded to search duration of 5 min) returned a DM shape enabling a Raman laser output power of 650 mW resulting in a power improvement of ~ 18 %. The beam quality M^2 factors along the x and y transverse axes were both measured less than 1.1 for the first Stokes laser output and 1.2 for the fundamental laser beam. Using a Shack-Hartman sensor, the wavefront correction induced by the DM shape before and after the search procedure was measured and the resulting Zernike coefficients are shown in Table 2.

Table 2. Zernike coefficients before and after power scaling investigation

Zernike coefficient order	starting point (μm)	end point (μm)	error range (μm)
1 (piston)	-18.59	-18.49	0.01
2 (tip y)	14.79	14.76	0.01
3 (tip x)	3.87	3.78	0.01
4 (astigmatism +/-45°)	0.019	0.016	0.002
5 (defocus)	-0.125	-0.118	0.002
6 (astigmatism +/-0°)	0.055	0.071	0.002
7 (trefoil y)	-0.001	-0.004	0.001
8 (coma x)	-0.004	-0.006	0.001
9 (coma y)	0.002	0.011	0.001
10 (trefoil x)	-0.002	-0.005	0.001

In addition to power scaling, this AO-based technique was also used as a mean to select the wavelength of the $Nd:YVO_4$ Raman laser. Neodymium-doped Ortho-Vanadates, such as $Nd:YVO_4$ and $Nd:GdVO_4$ have been shown to feature several Raman transitions [12] leading to the development of Raman lasers based on secondary Raman transitions [13-15]. Here, the AO-system was used to rapidly modify the dynamics of the intracavity laser field resulting in the switch between the primary (893 cm^{-1}) and secondary (379 cm^{-1}) Raman transitions of the

$Nd:YVO_4$ crystal. In this experiment, the laser cavity from Fig. 1 was slightly modified with the distance between the DM and the ROC = 1 m curved mirror set to 300 mm. At first, the laser resonator was manually aligned to only use the 379 cm^{-1} Raman shift with the DM actuators set at 0 V (i.e. focusing powers along the x and y axes measured at -0.47 D and -0.28 D respectively) resulting in a 275 mW Raman laser output at λ = 1109 nm for an absorbed laser diode pump power of 8.2 W. The beam quality M^2 factors along the x and y transverse axes were measured at 1.3 and 1.6 for the λ = 1109 nm laser output. Using an optical spectrum analyser (Agilent 86140B), the full width at half maximum (FWHM) linewidth of the first Stokes output (λ = 1109 nm) can be estimated at 0.15 nm with a resolution of 0.06 nm. The optical power transfer at λ = 1109 nm was measured as shown in Fig. 4. At a pump power of 10.1 W, ~ 100 mW of the λ = 1176 nm Raman output could also be observed in addition to the λ = 1109 nm line. The surface of the DM was then changed to a ~ flat shape by applying a voltage of 66 V to all actuators. In this way, the primary (893 cm^{-1}) Raman shift was favored to the detriment of the 379 cm^{-1} shift. So only the Raman laser at λ = 1176 nm could be observed with an output power of 340 mW and with beam quality M^2 factors along the x and y transverse axes measured at less than 1.1. The resulting FWHM linewidth of this Raman laser output was measured at 0.15 nm with a resolution of 0.06 nm. The optical power transfer of the λ = 1176 nm output obtained with a flat DM shape was measured as shown in Fig. 4. Again, at high pump powers (9.7 W), both Raman outputs could be observed with up to 100 mW of the λ = 1109 nm output. The Zernike coefficients before and after the wavelength switch are shown in Table 3.

Table 3. Summary of Zernike coefficients for wavelength control

Zernike coefficient order	starting point (µm)	end point (µm)
1 (piston)	-19.32	-18.99
2 (tip y)	15.38	15.06
3 (tip x)	3.77	3.83
4 (astigmatism+/-45°)	0.016	0.016
5 (defocus)	0.121	-0.013
6 (astigmatism+/-0°)	0.043	0.048
7 (trefoil y)	0.002	0.001
8 (coma x)	-0.001	-0.003
9 (coma y)	0.004	0.002
10 (trefoil x)	0.003	0.001

These two distinct experiments raise several discussion points.

Although the same DM was used in both investigations, the correction required to achieve the objective varied significantly. In the power scaling investigation, the correction range of the DM had to be limited to avoid any Raman laser modal collapse which can occur when a strong curvature change to the DM drives the laser cavity outside its stability range [8]. As seen in Table 2, high order correction (mainly astigmatism and coma) was required to optimise the Raman output power since the first order of the thermal lens had mainly been compensated using the pre-optimisation experiment. Meanwhile, in the wavelength selection experiment, a comparison of the Zernike coefficients expressed in Table 3 shows a significant variation in the defocus term (Z_5). Using this term along with the astigmatism term (Z_6), it is possible to calculate the radius of curvatures ROC_x and ROC_y of the DM shape as [16]:

$$Z_{5x} = Z_5 + \frac{Z_6}{\sqrt{2}} \tag{1}$$

$$Z_{5y} = Z_5 - \frac{Z_6}{\sqrt{2}} \tag{2}$$

$$ROC_x = \frac{-\Phi_x{}^2}{8\sqrt{3}\, Z_{5x}} \tag{3}$$

$$ROC_y = \frac{-\Phi_y{}^2}{8\sqrt{3}\, Z_{5y}} \tag{4}$$

where Z_{5x} and Z_{5y} denote the defocus term for the x and y axes and Φ_x and Φ_y are the diameter of the pupil along the x and y axes respectively (both diameters were 3 mm). Therefore, to favour the λ = 1109 nm output, the ROC of the DM surface along the x and y axes was measured at -4.29 m and -7.17 m respectively while to obtain the λ = 1176 nm line an ROCs of > 30 m and 13.8 m for the x and y axes were required respectively. Using an ABCD-matrix software, this cylindrical curvature variation of the DM surface was found to increase the fundamental transverse mode of the λ = 1064 nm laser in the gain medium by ~ 15 %. So it can be concluded that, optimal power scaling would require a DM with a moderate stroke and a large number of actuators whereas wavelength selection could be best achieved using a DM with a lower number of actuators and a larger stroke.

In Fig. 3, the power transfer recorded prior to Raman output power optimisation displays a distinct rollover commensurate with thermal lensing at pump powers above 10.4 W. The optimised Raman laser output power recorded for a pump power of 10.8 W is in line with the linear trend displayed for lower pump powers. Therefore, the disappearance of the rollover behaviour makes us believe that the AO-control loop has significantly reduced the effect of thermal lensing within the $Nd:YVO_4$ crystal. In addition, the use of a bespoke random search algorithm was an attempt to conciliate speed with performance. More advanced algorithms will be required to improve the efficacy of this feedback loop.

In the wavelength control investigation, both Raman outputs could be simultaneously observed at pump powers above 9.5 W. Further investigation would be required to explain this Raman mode competition. However, it must be noted that the sum of their intensity meant that the total Raman output power was in line with the trend observed from lower powers.

In conclusion, for the first time to our knowledge, intracavity adaptive optics was implemented inside a solid-state Raman laser to automatically increase the power and control the wavelength of the Raman output beam. The feedback control loop used for power scaling featured a DM, a photodiode sensor and a pc-based control program using a random search algorithm. The use of this control loop resulted in an 18 % improvement of the Raman laser output power of an end-pumped Nd:YVO_4 self-Raman laser emitting at $\lambda = 1176$ nm. This proof-of-context experiment demonstrates the potential of intracavity AO to alleviate the detrimental effects of thermal lensing and open avenues for power scaling of CW and high average power crystalline Raman lasers. In addition, wavelength control between $\lambda = 1109$ nm and $\lambda = 1176$ nm has been achieved using this AO technique based on the 379 cm^{-1} and 893 cm^{-1} Raman shift of YVO_4. This experiment paves the way towards automatic wavelength selectable high power Raman lasers.

This work has been supported by the UK EPSRC (Grant number EP/K009982/1).

References

1. P. Cerny, H. Jelinkova, P. G. Zverev, T. T. Basiev, Prog. Quantum Electron. **28**, 113-143 (2004).
2. J. A. Piper and H. M. Pask, IEEE J. Sel. Top. Quantum Electron. **13**, 692–704 (2007).
3. H. M. Pask, P. Dekker, R. P. Mildren, D. J. Spence, J. A. Piper, Prog. Quantum Electron. **32**, 121–158 (2008).
4. A. J. Lee, H. M. Pask, D. J. Spence, and J. A. Piper, Opt. Lett. **35**, 682–684 (2010).
5. W. Lubeigt, G. M. Bonner, J. E. Hastie, M. D. Dawson, D. Burns, and A. J. Kemp, Opt. Lett. **35**, 2994-2996 (2010).
6. V. G. Savitski, I. Friel, J. E. Hastie, M. D. Dawson, D. Burns, and A. J. Kemp, IEEE J. of Quantum Electron., **48**, 328-337 (2012).
7. O. Kitzler, A. McKay, and R. P. Mildren, Opt. Lett. **37**, 2790-2792 (2012).
8. W. Lubeigt, G. Valentine and D. Burns, Opt. Express. **16**, 10943-10955 (2008).
9. P. Yang, X. Lei, R. Yang, M. Ao, L. Dong, B. Xu, Appl. Phys. B **100**, 591-595 (2010).
10. S. Piehler, B. Weichelt, A. Voss, M. A. Ahmed, and T. Graf, Opt. Lett. **37**, 5033-5035 (2012).
11. W. Lubeigt, S. P. Poland, G. J. Valentine, A. J. Wright, J. M. Girkin, and D. Burns, Appl. Opt. **49**, 307-314 (2010).
12. A. A. Kaminskii, K. Ueda, H. J. Eichler, Y. Kuwano, H. Kouta, S. N. Bagaev, T. H. Chyba, J. C. Barnes, G. M. A. Gad, T. Murai, and J. Lu, Opt. Commun. **194**, 201–206 (2001).
13. F. Shuzhen, Z. Xingyu, W. Qingpu, L. Zhaojun, L. Lei, C. Zhenhua, C. Xiaohan, Z. Xiaolei, Opt. Commun. **284**, 1642–1644 (2011).
14. J. Lin and H. M. Pask, Opt. Express **20**, 15180–15185 (2012).
15. R. Li, R. Bauer, and W. Lubeigt, Opt. Express **21**, 17745-17750 (2013).
16. D. Malacara, *Optical Shop Testing, 2nd ed.* (John Wiley & Sons, 1992).

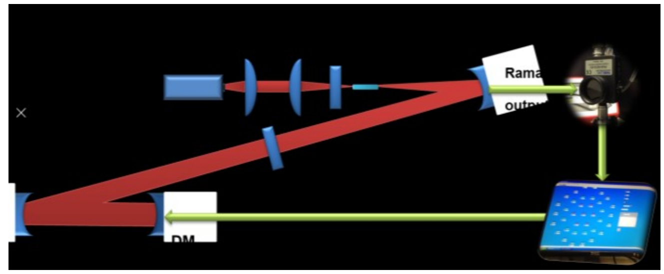

Fig. 1. Diagram of the Nd:YVO_4 self-Raman laser incorporating the AO feedback loop.

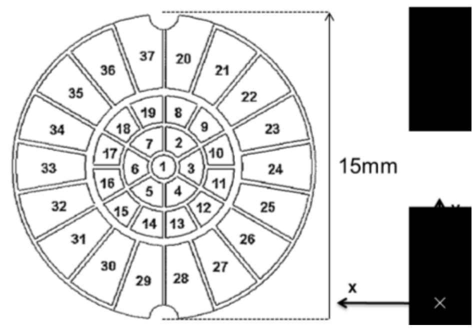

Fig. 2. Actuator designation of deformable mirror.

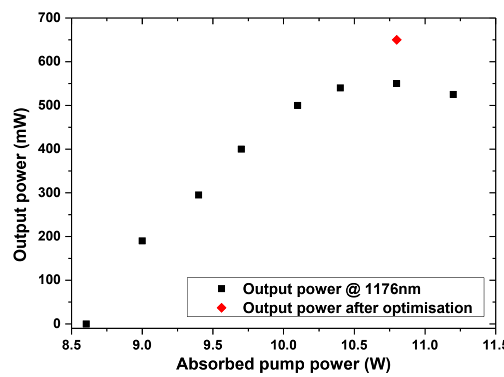

Fig. 3. Power transfer of the λ = 1176nm output before optimization including the post-optimisation result.

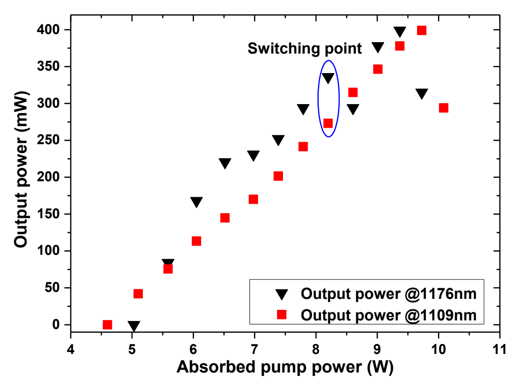

Fig. 4. Power transfer of Raman lasers resulting from the 379cm-1 transition (in red) and the 893cm-1 transition (in black).

References

1. P. Cerny, H. Jelinkova, P. G. Zverev, and T. T. Basiev, "Solid state lasers with Raman frequency conversion," Prog. Quantum Electron. **28**, 113-143 (2004).

2. J. A. Piper and H. M. Pask, "Crystalline Raman lasers," IEEE J. Sel. Top. Quantum Electron. **13**(3), 692-704 (2007).

3. H. M. Pask, P. Dekker, R. P. Mildren, D. J. Spence, and J. A. Piper, "Wavelength-versatile visible and UV sources based on crystalline Raman lasers," Prog. Quantum Electron. **32**, 121-158 (2008).

4. A. J. Lee, H. M. Pask, D. J. Spence, and J. A. Piper, "Efficient 5.3 W cw laser at 559 nm by intracavity frequency summation of fundamental and first-Stokes wavelengths in a self-Raman Nd:$GdVO_4$ laser," Opt. Lett. **35**(5), 682-684 (2010).

5. W. Lubeigt, G. M. Bonner, J. E. Hastie, M. D. Dawson, D. Burns, and A. J. Kemp, "Continuous-wave diamond Raman laser," Opt. Lett. **35**(17), 2994-2996 (2010).

6. V. G. Savitski, I. Friel, J. E. Hastie, M. D. Dawson, D. Burns, and A. J. Kemp, "Characterization of Single-Crystal Synthetic Diamond for Multi-Watt Continuous-Wave Raman Lasers," IEEE J. of Quantum Electron., **48**(3), 328-337 (2012).

7. O. Kitzler, A. McKay, and R. P. Mildren, "Continuous-wave wavelength conversion for high-power applications using an external cavity diamond Raman laser," Opt. Lett. **37**(14), 2790-2792 (2012).

8. W. Lubeigt, G. Valentine and D. Burns, "Enhancement of laser performance using an intracavity deformable membrane mirror," Opt. Express. **16**(15), 10943-10955 (2008).

9. P. Yang, X. Lei, R. Yang, M. Ao, L. Dong, B. Xu, "Fast and stable enhancement of the far-field peak power by use of an intracavity deformable mirror," Appl. Phys. B **100**, 591-595 (2010).

10. S. Piehler, B. Weichelt, A. Voss, M. A. Ahmed, and T. Graf, "Power scaling of fundamental-mode thin-disk lasers using intracavity deformable mirrors," Opt. Lett. **37**(24), 5033-5035 (2012).

11. W. Lubeigt, S. P. Poland, G. J. Valentine, A. J. Wright, J. M. Girkin, and D. Burns, "Search-based active optic systems for aberration correction in time-independent applications," Appl. Opt. **49**(3), 307-314 (2010).

12. A. A. Kaminskii, K. Ueda, H. J. Eichler, Y. Kuwano, H. Kouta, S. N. Bagaev, T. H. Chyba, J. C. Barnes, G. M. A. Gad, T. Murai, and J. Lu, "Tetragonal vanadates YVO_4 and $GdVO_4$ – new efficient $\chi_{(3)}$ - materials for Raman lasers," Opt. Commun. **194**, 201–206 (2001).

13. F. Shuzhen, Z. Xingyu, W. Qingpu, L. Zhaojun, L. Lei, C. Zhenhua, C. Xiaohan, Z. Xiaolei, "1097 nm Nd:YVO4 self-Raman laser," Opt. Commun. **284**, 1642–1644 (2011).

14. J. Lin and H. M. Pask, "Cascaded self-Raman lasers based on 382 cm^{-1} shift in Nd:$GdVO_4$.," Opt. Express **20**(14), 15180–15185 (2012).

15. R. Li, R. Bauer, and W. Lubeigt, "Continuous-Wave Nd:YVO_4 self-Raman lasers operating at 1109nm, 1158nm and 1231nm," Opt. Express **21**(15), 17745-17750 (2013).

16. D. Malacara, *Optical Shop Testing, 2nd ed.* (John Wiley & Sons, 1992).